CHARACTERIZATION OF LONGITUDINAL ELECTRON BEAM QUALITY AT THE SOFT X-RAY BEAMLINE OF SwissFEL

R. Provvedi*, E. Prat, S. Reiche
PSI Center for Accelerator Science and Engineering, Villigen, Switzerland

Abstract

Longitudinal electron beam quality is key at X-ray free-electron lasers (FELs), where electron beams with small slice energy spread and a well-preserved current profile are required to ensure optimal, stable performance. Collective effects such as microbunching instability (MBI) and intrabeam scattering (IBS) can significantly degrade the longitudinal phase-space of the electron beam during multi-stage compression and are therefore a concern across FEL facilities. In this contribution, we will present systematic characterization studies of these mechanisms at the SwissFEL soft X-ray beamline Athos. We will show longitudinal phase-space measurements using radiofrequency transverse-deflecting structures for different accelerator and compression conditions. These characterization studies represent a first step towards the optimization of multi-stage compression schemes aimed at mitigating MBI and IBS effects.

INTRODUCTION

X-ray free-electron lasers (XFELs) are powerful light sources delivering ultrashort, high-brilliance X-ray pulses with atomic-scale spatial and femtosecond temporal resolution [1]. The performance of the FEL amplification process is critically dependent on the quality of the driving electron beam, in particular on its longitudinal phase space (LPS). To achieve the high peak currents required for efficient FEL operation, electron bunches undergo multiple stages of longitudinal compression along the accelerator lattice. While this process is essential for maximizing FEL gain, it concurrently enhances collective effects that can severely degrade the beam quality, thereby limiting the achievable gain and spectral purity, particularly in seeded FEL configurations. Among the effects arising from beam self-interactions, intrabeam scattering (IBS), i.e., multiple Coulomb scattering events, leads to a growth of the uncorrelated energy spread. In contrast to storage rings, the beam in a linear accelerator is not in thermal equilibrium and typically exhibits a higher effective transverse than longitudinal temperature. As a consequence, IBS drives a redistribution of the phase-space density with a net transfer of momentum from the transverse to the longitudinal degrees of freedom, resulting in an energy spread growth [2]. Microbunching instability (MBI), in contrast, is characterized by the amplification of the initial density and energy modulations over a broad wavelength spectrum, primarily driven by longitudinal space-charge (LSC) forces and coherent synchrotron radiation (CSR), during bunch compression and dispersive transport [3, 4].

* roberta.provvedi@psi.ch

The SwissFEL facility [5, 6] at the Paul Scherrer Institute (PSI) in Villigen, Switzerland, delivers X-ray radiation through two beamlines, namely Aramis, serving the hard X-ray regime, and Athos, dedicated to soft X-ray production. The latter operates over a wavelength range of 0.65–5.0 nm and is tailored for flexible operating modes, polarization control, and advanced seeding schemes, thereby placing stringent requirements on the longitudinal beam quality. A characterization of the LPS evolution along the accelerator is therefore needed to understand and control the impact of collective effects. In this work, experimental studies of the longitudinal beam quality at SwissFEL Athos are presented, combining high-resolution measurements with ongoing simulation studies. Emphasis is placed on different bunch compression schemes to investigate how IBS- and MBI-driven effects manifest under varying compression and to distinguish the corresponding operational regimes.

LPS DIAGNOSTICS

Measurements

The longitudinal phase space (LPS) of the electron beam at SwissFEL is experimentally characterized using radiofrequency (RF) transverse deflecting structures (TDS) in combination with a two-dimensional profile monitor located in a downstream dispersive section. The TDS imparts a time-dependent transverse kick to the electron bunch, mapping the longitudinal coordinate onto one transverse screen axis, while the relative energy deviation is encoded along the orthogonal axis via the local dispersion. The temporal coordinate is calibrated using the applied TDS voltage and phase, whereas the energy scale is determined from the dispersion at the observation screen. SwissFEL is equipped with multiple TDS systems with different frequencies and resolutions: an S-band TDS (3 GHz, ~10 fs resolution) at the injector, a C-band TDS (5.7 GHz, ~1 fs) downstream of Linac 3 and an X-band TDS (12 GHz, <1 fs) installed after the Athos undulator. A schematic layout of the SwissFEL accelerator lattice, including the relevant diagnostic, is shown in Fig. 1.

This diagnostic setup enables direct, single-shot LPS measurements with femtosecond temporal resolution. From the LPS distributions, several key parameters can be extracted, namely the current profile, energy centroid and slice energy spread (SES) as function of the longitudinal coordinate, as well as the energy chirp along the bunch. To ensure a systematic and reproducible analysis of the measured data, a dedicated analysis framework (MBI Analyzer Tool) has been developed. It processes LPS images acquired from the diagnostic screens and reconstructs slice-resolved beam properties along the bunch. Noise reduction is performed using

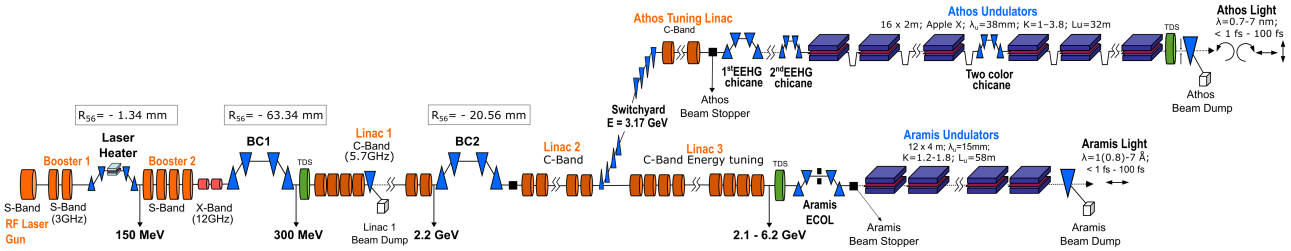

Figure 1: Schematic layout of the SwissFEL accelerator lattice, including magnetic bunch compressors, RF accelerating cavities and relevant diagnostics. Beam stoppers, dumps and transverse-deflecting structures (TDS) are indicated.

adaptive masking techniques to suppress uncorrelated background contributions. Subsequent spectral analysis of the two-dimensional longitudinal beam structure is performed using Fast Fourier Transform (FFT) techniques. By combining time-resolved LPS reconstruction with frequency-domain analysis, high-frequency density and energy modulations can be quantified, providing access to the spectral content of the beam. These features are characteristic signatures of the development of the microbunching instability and can be quantified in terms of their wavelength, amplitude, and gain curves, enabling a comprehensive characterization of the MBI-induced microstructures. The experimental studies presented in the following sections investigate IBS- and MBI-driven phase-space evolution at SwissFEL under multiple compression schemes.

Simulations

Start-to-end simulations are ongoing to support the experimental observations. The LPS evolution along the accelerator is simulated with ELEGANT [7], using initial beam distributions at the SwissFEL injector generated with ASTRA code [8]. Particle tracking in ELEGANT is used to model beam acceleration, compression, and transport, providing sliced beam parameters along the machine. IBS and MBI are not treated self-consistently but are accounted for through simplified analytical models within a partially decoupled framework. This approach is justified by their negligible impact on the macroparticle trajectories in the considered regime, while their cumulative effect on the longitudinal beam dynamics can be captured using reduced models. MBI dynamics is described using a one-dimensional linear model based on the Bosch–Kleman formalism [9], tracking the evolution of the bunching factor $b(k)$ and the corresponding energy modulation $\delta\gamma(k)$ along the lattice, where k denotes the modulation wavenumber. LSC-driven amplification of energy modulations is included via an effective impedance, while CSR effects in chicanes are negligible under typical SwissFEL operating conditions. IBS-induced energy spread growth is modeled using Piwinski theory [2] and incorporated stepwise into the uncorrelated energy spread to account for the additional Landau damping arising from IBS.

RESULTS

Single-stage Compression Studies

Systematic LPS measurements were performed in a single-stage bunch compression configuration, with only the first bunch compressor (BC1) operated in dispersive mode (R_{56} = 63.34 mm). The beam peak current was scanned from 95 A up to ~1.4 kA by varying the compression strength in BC1. Observations were carried out at different locations along the accelerator, namely downstream of the injector and at the end of Linac 3. In order to enhance the resolution of the relative slice energy spread measurements, the beam energy at the exit of Linac 3 was reduced to approximately 2.7 GeV. Representative LPS measurements acquired downstream of the injector and at the end of Linac 3 are shown in Fig. 2, for two peak current values of approximately 95 A and 145 A. The measured energy spread growth at the injector as a function of peak current is consistent with the expected IBS scaling, i.e., $d\sigma_\gamma^2/dz \propto I\gamma^{1/2}\varepsilon_n^{-3/2}\beta^{-1/2}$, integrated piecewise, in agreement with previous studies at SwissFEL [10]. In contrast, measurements downstream of Linac 3 significantly exceed the expected IBS scaling, indicating a non-negligible contribution of MBI to the beam energy spread, at frequencies that cannot be resolved by the TDS measurements. Ongoing simulations aim to confirm and quantify the respective contributions of IBS and MBI.

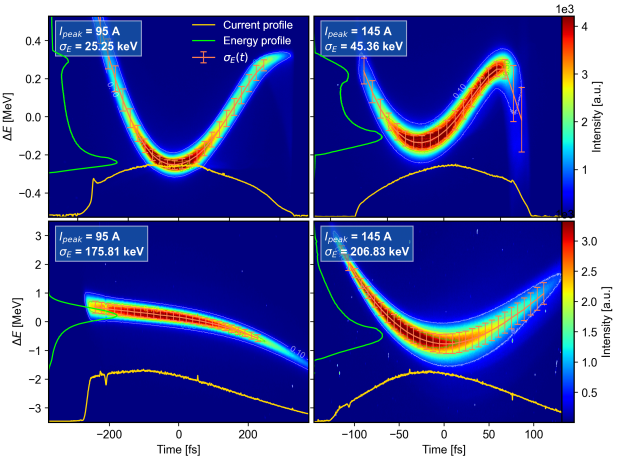

Figure 2: LPS measurements downstream of the injector (top) and at the end of Linac 3 (bottom) for different beam peak currents in single-stage bunch compression.

Multi-stage Compression Studies at Athos

The investigation was extended to multi-stage compression configurations involving BC1 (R_{56} = 63.34 mm), BC2 (R_{56} = 20.56 mm), and the Athos switchyard as dispersive transport line, with LPS diagnostics performed at the Athos

beam dump. Compared to the single-stage compression, pronounced distortions of the LPS and an increase in SES are observed, as shown in Fig. 3. These features indicate the onset of collective effects beyond IBS, with high-frequency longitudinal structures consistent with MBI development.

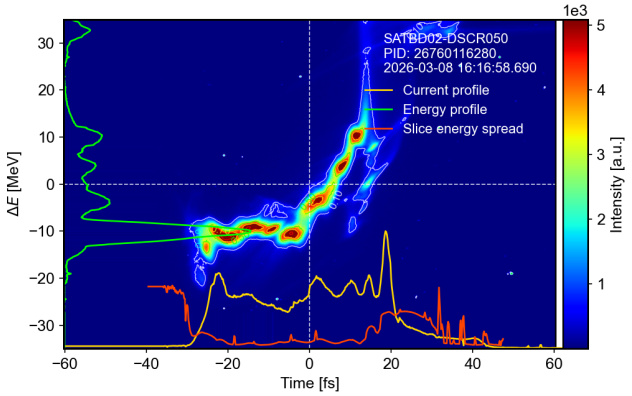

Figure 3: Electron beam LPS measured at the Athos beam dump under four-stage compression.

To investigate MBI under controlled conditions, dedicated measurements were performed by scanning the longitudinal dispersion R_{56} of a small EEHG chicane located in the Athos beamline. The chicane strength was varied by adjusting the dipole currents from 0 A to 140 A in steps of 10 A, corresponding to R_{56} values ranging from 0 up to ~ 400 μm. For each machine setting, stacks of 50 LPS images were acquired to ensure statistical robustness. Measurements were performed for two beam configurations: a nominal beam with rms bunch length of 20.21 ± 0.70 fs and a decompressed beam of 45.89 ± 0.89 fs. The scanned R_{56} enables controlled LPS manipulation, modifying both the coupling between energy and density modulations, and the damping of high-frequency components through the finite SES. Considering the definition of the *bunching spectrum* as the Fourier transform of the density modulation, i.e., $B(f) \equiv \mathcal{F}\{\delta b(t)\}$, $S_b(f) = |B(f)|^2$ represents the spectral power of the longitudinal density modulations and provides an experimental measure of microbunching strength as a function of longitudinal wavelength. Figure 4 shows the dominant microbunching wavelengths and normalized microbunching amplitude $A_{\mathrm{MBI}} \equiv \max[S_b(f)]/\langle S_b(f)\rangle$ as function of the chicane R_{56}. Up to a normalization factor, A_{MBI} is proportional to $|b(k)|^2$. A reduction of the microbunching amplitude is observed at specific R_{56} values, indicating the existence of operating conditions where partial suppression of MBI can be achieved through an appropriate tuning of the local dispersive strength. This behaviour can be understood in terms of a reduction of the first term in square brackets in the linearized expression for the bunching factor downstream of a dispersive section [3]:

$$b_f(k_d) \simeq \left[b_i(k) - ik_d R_{56} \frac{\delta\gamma_i(k)}{\gamma} \right] \exp\left[-\frac{1}{2} \left(k_d R_{56} \frac{\sigma_\gamma}{\gamma} \right)^2 \right]$$

where $b_i(k)$ is the upstream bunching factor, $\delta\gamma_i(k)$ the energy modulation, $k_d = Ck$ and σ_γ the uncorrelated energy

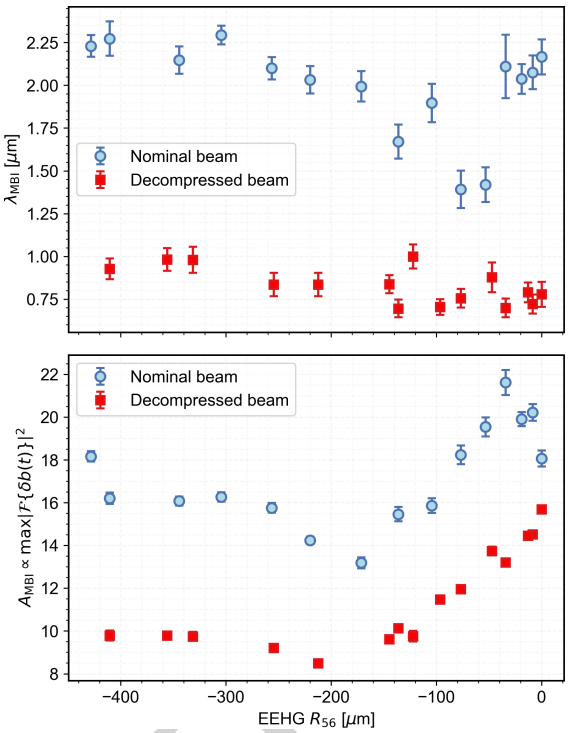

Figure 4: Dominant microbunching wavelength (top) and amplitude (bottom) versus the EEHG chicane strength.

spread. By properly tuning R_{56}, it is possible to reduce the cumulative microbunching amplification over the distance between nominal compression stages for the most critical frequencies, without degrading the 6D beam brightness. This suggests that small dispersive chicanes inserted between compression stages could provide an effective strategy for mitigating the microbunching instability.

CONCLUSIONS AND OUTLOOK

This work establishes a consistent experimental framework for investigating IBS and MBI at SwissFEL, providing quantitative benchmarks for analytical models and start-to-end simulations. Initial experimental and numerical characterization of the longitudinal electron beam properties has been presented. Multi-stage compression schemes exhibit clear signatures of MBI-induced density modulations. By scanning the dispersion upstream of the Athos undulator, a systematic evolution of the microbunching features and beam spectral content is observed, depending on the compression settings. The measurements indicate a strong sensitivity of the instability dynamics to dispersive optics and show that the microbunching amplification can be partially mitigated through appropriate tuning of the compression parameters. Future work will focus on comparisons with macroparticle tracking codes and advanced analytical MBI models, as well as on the systematic optimization of multi-stage compression schemes aimed at reducing the impact of MBI on the FEL spectrum. Further studies will also address the role of the multi-bend switchyard in the instability evolution, which is expected to enhance MBI through the amplification of residual density and energy modulations exiting the linac.

REFERENCES

[1] Z. Huang and K.-J. Kim, "Review of x-ray free-electron laser theory", *Phys. Rev. Accel. Beams*, vol. 10, p. 034801, 2007. doi:10.1103/PhysRevSTAB.10.034801

[2] A. Piwinski, "Intra-beam-scattering", in *Proc. 9th Int. Conf. on High-Energy Accelerators*, pp. 405–409, May 1974. doi:10.5170/CERN-1992-001.226

[3] Z. Huang and K.-J. Kim, "Formulas for coherent synchrotron radiation microbunching in a bunch compressor chicane", *Phys. Rev. Spec. Top. Accel. Beams*, vol. 5, p. 074401, 2002. doi:10.1103/PhysRevSTAB.5.074401

[4] S. Heifets, G. Stupakov, and S. Krinsky, "Coherent synchrotron radiation instability in a bunch compressor", *Phys. Rev. Spec. Top. Accel. Beams*, vol. 5, p. 064401, 2002. doi:10.1103/PhysRevSTAB.5.064401

[5] E. Prat *et al.*, "A compact and cost-effective hard x-ray free-electron laser driven by a high-brightness and low-energy electron beam", *Nat. Photonics*, vol. 14, pp. 748–754, 2020. doi:10.1038/s41566-020-00712-8

[6] E. Prat *et al.*, "An x-ray free-electron laser with a highly configurable undulator and integrated chicanes for tailored pulse properties", *Nat. Commun.*, vol. 14, p. 5069, 2023. doi:10.1038/s41467-023-40759-z

[7] M. Borland, "elegant: A Flexible SDDS-Compliant Code for Accelerator Simulation", in *Proc. 6th Int, Comput. Accel. Phys. Conf. (ICAP'00)*, 2000. doi:10.2172/761286

[8] K. Floettmann, "ASTRA: A Space Charge Tracking Algorithm", DESY, Hamburg, Germany, Mar. 2017, https://www.desy.de/~mpyflo/Astra_manual/Astra-Manual_V3.2.pdf

[9] R. A. Bosch and K. J. Kleman, "Modeling Two-Stage Bunch Compression with Wakefields: Macroscopic Properties and Microbunching Instability", *Phys. Rev. Spec. Top. Accel. Beams*, vol. 11, no. 9, p. 090702, 2008. doi:10.1103/PhysRevSTAB.11.090702

[10] E. Prat *et al.*, "Energy spread blowup by intrabeam scattering and microbunching at the SwissFEL injector", *Phys. Rev. Accel. Beams*, vol. 25, p. 104401, 2022. doi:10.1103/PhysRevAccelBeams.25.104401